remote sensing

MDPI

Supplementary material

Towards Unified Online-Coupled Aerosol Parameterization for the Brazilian Global Atmospheric Model (BAM): Aerosol–Cloud Microphysical–Radiation Interactions

Jayant Pendharkar [1], Silvio Nilo Figueroa [1], Angel Vara-Vela [2,3,4], R. Phani Murali Krishna [5], Daniel Schuch [6], Paulo Yoshio Kubota [1], Débora Souza Alvim [1,7], Eder Paulo Vendrasco [1], Helber Barros Gomes [8], Paulo Nobre [1] and Dirceu Luís Herdies [1,*]

[1] National Institute for Space Research (INPE), Cachoeira Paulista, São José dos Campos 12227-010, SP, Brazil
[2] Department of Geoscience, Aarhus University, 8000 Aarhus, Denmark
[3] Department of Physics and Astronomy, Aarhus University, 8000 Aarhus, Denmark
[4] iCLIMATE Aarhus University Interdisciplinary Centre for Climate Change, Aarhus University, 4000 Roskilde, Denmark
[5] Indian Institute of Tropical Meteorology, Pune 411008, India
[6] Department of Civil and Environmental Engineering, Northeastern University, Boston, MA 02115, USA
[7] Lorena School of Engineering (EEL), University of Sao Paulo (USP), Lorena 12602-810, SP, Brazil
[8] Institute of Atmospheric Sciences, Federal University of Alagoas, Maceio 57072-900, AL, Brazil
* Correspondence: dirceu.herdies@inpe.br

Contains:

Table S1. Aerosol and their effects on climate. Column 1 lists the aerosol species. Column 2 lists the physical processes pertaining to the species. The uncertainties in the estimation of radiative forcings or burdens are listed in Column 3. Models and the preferred mode of coupling corresponding to the results in column 3 are listed in Column 4. The references are listed in column 5.

Species (effect on climate)	Physical processes	Uncertainty in radiative forcings or burden	Models (configuration)	Ref.
Carbonaceous (warming)	absorption of solar radiation, condensation and coagulation (transform to hydrophilic), nucleation, wet scavenging	direct radiative forcing of internally mixed BC twice as large as externally mixed.	online-coupled – GATOR-GCMM[a], GISS GCM II'[b]	[9-11]
		negative radiative forcing.	offline – GRANTOUR/CCM[c]	[12]
Sulfate (cooling)	scattering solar radiation, condensation, homogeneous nucleation, wet scavenging	variations in the predicted indirect radiative forcings ranging from − 0.4 Wm^{-2} to − 1.7 Wm^{-2} depending upon the empirical relation used.	online-coupled – based on empirical relation between CDNC and sulfate mass (ECMWF[d], NCAR-CCM3[e]); and – based on physically based parameterization (ECMWF, MIRAGE[f])	[13-15] [16-17]
SOA (net cooling)	Absorption and scattering of solar radiation, new particle formation, heterogeneous chemistry, growth	global SOA budget (12 – 1820 Tg yr^{-1}); direct forcing − 0.26 to − 0.77 Wm^{-2}; indirect forcings − 0.6 to − 0.77 Wm^{-2}.	online-coupled – GLOMAP[g], NCAR-CAM5[h]; sensitive to anthropogenic and biogenic precursor emissions, and formation pathways.	[19-21]
Dust (net cooling)	Absorption and scattering of solar radiation, nucleation, heterogeneous reactions altering	emission factors vary by a factor of 2, radiative forcing at the top of atmosphere (− 0.16 Wm^{-2} to − 0.92	online-coupled – NCAR-CCSM3-CLM3[i], GOCART[j], NASA-GISS[k], HadGCM[l],	[22-33]

	photolysis rates, transport, dry and wet deposition	Wm^{-2}) is different from the surface (– 1.22 Wm^{-2} to − 1.82 Wm^{-2}), localized sources but are transported to long distance.	offline – MATCH-DEAD[m]	
Seasalt (cooling)	Scattering of solar radiation, nucleation, growth, dry and wet deposition and transport	Global budget varies between 1000 and 3000 Tg yr^{-1}, complex production mechanism given the wide size range and lifetimes.	Canadian GCM, NCAR-CAM5, ECMWF	[34-38]

[a] Gas, Aerosol, Transport, Radiation, General Circulation, and Mesoscale Meteorological model.
[b] Goddard Institute for Space Studies General Circulation Model II-prime.
[c] Lawrence Livermore National Laboratory tropospheric chemistry model with a GCM.
[d] European Centre for Medium Range Weather Forecasts
[e] National Center for Atmospheric Research – Community Climate Model
[f] Model for Integrated Research on Atmospheric Global Exchange
[g] Global Model of Aerosol Processes
[h] Community Atmosphere Model version 5
[i] NCAR Community Climate System Model – Community Land Model
[j] Goddard Chemistry Aerosol Radiation and Transport
[k] NASA Goddard Institute for Space Sciences ModelE
[l] Hadley Centre atmospheric general circulation model
[m] Dust Entrainment and Deposition Model – Model of Atmospheric Transport and Chemistry

Table S2. List of acronyms

Acronym	Expansion
ACCMIP	Atmospheric Chemistry and Climate Model Intercomparison Project
AOD	aerosol optical depth
AMIC	aerosol microphysics
ASY	asymmetry parameter
BAM	Brazilian global atmospheric model
BC	black carbon
BESM	Brazilian Earth System Model
CAM5-MAM3	Community Atmosphere Model-Modal Aerosol Model
CCN	cloud condensation nuclei
CDNC	cloud droplet number concentration
CERES	Clouds and Earth's Radiant Energy System
CLDF	cloud fraction
CO	Carbon Monoxide
COD	cloud optical depth
CPTEC	Centre for Weather Forecast and Climate Studies
CTRL	Control
SMT	smooth topography
D_{gN}	geometric mean diameter
DMS	dimethyl sulfide
DU	Dust
ECHAM-HAM	European Centre Hamburg Model-Hamburg Aerosol Model
EDGAR	Emissions Database for Global Atmospheric Research
FINN	Fire INventory from NCAR
FRM	Fire Radiative Power
GCM	general circulation model
GPCP	Global Precipitation Climatology Product
H_2O_2	hydrogen peroxide
H_2SO_4	sulfuric acid
IBIS	Integrated Biosphere Simulator
IN	ice nuclei
ITCZ	Inter Tropical Convergence Zone
JFM	January--March
JAS	July--September
LW	longwave
LWCRF	longwave cloud radiative forcings
LWP	liquid water path
MEGAN	Model of Emissions of Gases and Aerosols from Nature
MIRAGE	Model for Integrated Research on Atmospheric Global Exchanges
MODIS	Moderate Resolution Imaging Spectroradiometer
NCAR	National Center for Atmospheric Research

NH	northern hemisphere
NH_3	ammonia
NMB	normalized mean bias
OC	organic carbon
OLR	outgoing longwave radiation
PNNL	Pacific Northwest National Laboratory
POM	primary organic matter
QFED	Quick Fire Emission Database
R	Pearson's correlation coefficient
RMSE	root mean square error
RRTMG	Rapid Radiative Transfer Model for GCM
SA	South America
SH	southern hemisphere
SMT	smooth topography
SOA	Secondary organic aerosol
SOAG	semi-volatile organic species
SO_2	sulfur dioxide
SS	seasalt
SSA	single-scattering albedo
SW	shortwave
SWCRF	shortwave cloud radiative forcings
SWDOWN	downward shortwave
S2S	subseasonal-to-seasonal
TOA	top of the atmosphere
VOC	volatile organic compound
WRF-Chem	Weather Research and Forecasting - Chemistry

Cloud microphysical properties

We examined the framework of AMIC in BAM subjected to incoming emissions and forcings in Figures 2 and 3. Next, we analyze its influence on clouds. The column droplet number concentration averaged for both seasons is shown in Figure S1. For JFM2014, the range varies from 52 to 3.78×10^6 m^{-2} with global mean of 2×10^5 m^{-2}. Significant concentrations are seen over land masses at high latitudes in the NH. For example, concentrations above 2.5×10^6 m^{-2} are seen over Europe and parts of western Russia, followed by North America and Canada. Over the biomass burning regions in Central Africa and outflow areas, concentrations of about 2×10^5 m^{-2} are seen (Figure S1). Concentrations in regions over the ocean at high latitudes in both hemispheres can be attributed to SS emissions due to high wind speeds. During the peak biomass burning season in SA (JAS2019 experiment), concentrations up to 7×10^5 m^{-2} are seen over the continent with significant contributions over the Amazon, eastern part of Brazil, over SA peak over La Plata basin, which stretches from northeastern Argentina to south-southeastern Brazil and receives heat, moisture, and biomass-burning products from the Amazon all year. As a consequence, destructive hailstorms are often observed over this mountainous region during late winter and early spring, between September and October [103]. Over remote oceans, SS emissions lead to formation of Aitken mode particles and CCN production. Sulfate forms CCN whose increase produces higher CDNC leading to smaller cloud droplet radii thereby enhancing scattering and thus cloud albedo. The global mean CCN concentrations for JFM2014 and JAS2019 are 1337 and 1241 cm^{-3} respectively (Table 2).

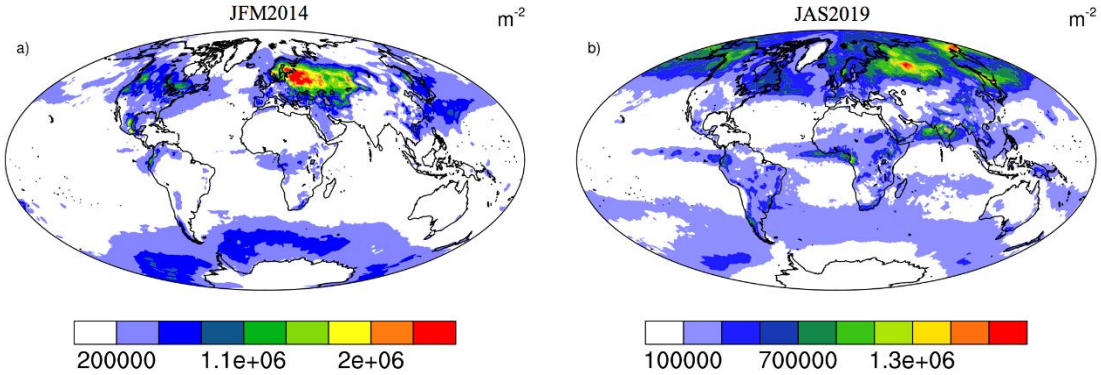

Figure S1. Vertically integrated column droplet number concentration (per m^2) averaged for the periods – a) JFM2014 and b) JAS2019 in BAM AMIC experiments.

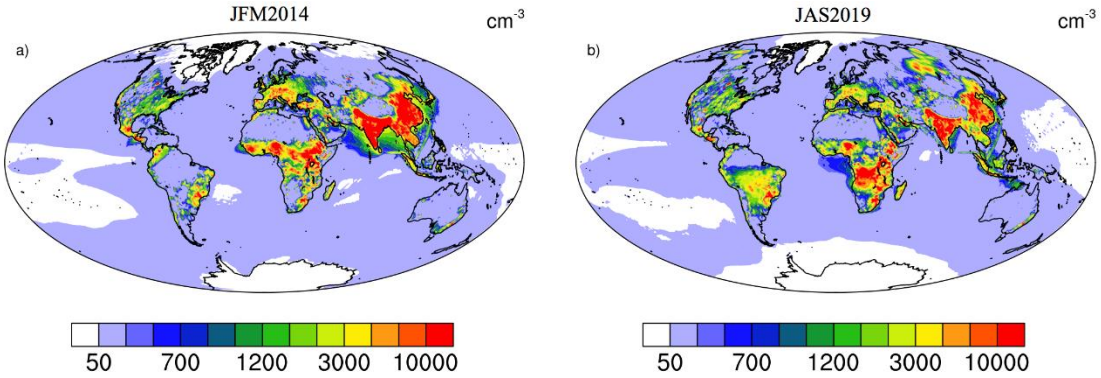

Figure S2. Surface concentration (per cm^3) of CCN at 0.5% supersaturation averaged for the periods – a) JFM2014 and b) JAS2019 in BAM AMIC experiments.

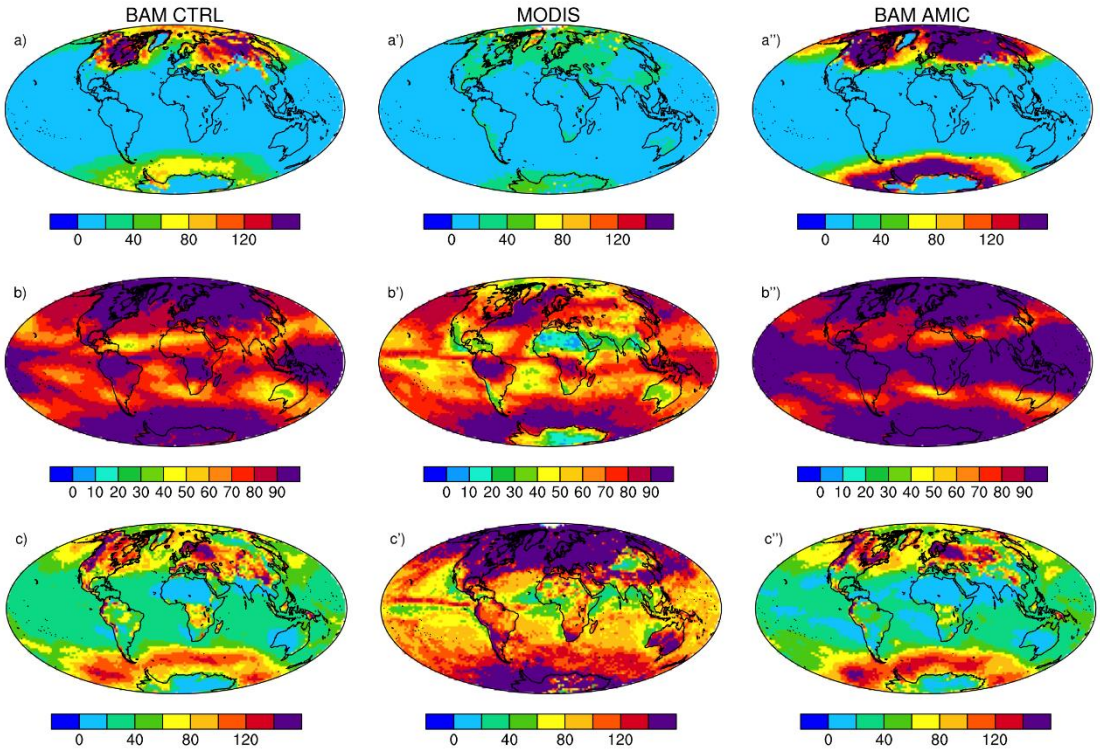

Figure S3. a: Model evaluation of cloud optical properties for JFM2014. Simulated JFM means from BAM CTRL (left column) and BAM AMIC (right column) are compared with MODIS satellite observations (middle column) corresponding to similar period. Variables evaluated include

[a,a′,a″] shortwave cloud optical depth (COD); [b,b′,b″] cloud fraction (CLDF) in %; and [c,c′,c″] cloud liquid water path (LWP) in g m^{-2}.

Figure S3a shows a comparison of BAM CTRL and BAM AMIC simulated JFM averages of shortwave cloud optical depth, cloud fraction, and cloud liquid water path with MODIS observations. Compared to observations, the simulated CLDF (b,b′,b″) are largely overpredicted in experiments with and without aerosols, specifically over the higher latitudes in both hemispheres that can relate to higher CDNCs simulated over those regions. Relatively, the inclusion of aerosols in BAM increased the cloud cover, with a large overprediction in the tropics. The NMBs lie within 10% for simulations with (42%) and without (33%) aerosols. Similar to CLDF, simulated COT (a,a′,a″) are overpredicted with large NMBs (122 and 367%) and RMSEs (59.71 and 137.36). Spatial patterns of COD are mostly similar in both simulations, except that the magnitudes scale up due to the presence of aerosols. Differing from the CLDF and COD patterns, simulated LWP (in g m^{-2}) is underpredicted with NMBs of −54% (without aerosols) and −46% (with aerosols) and corresponding RMSEs of 168 and 161.4, respectively. For the second set of experiments (JAS2019), Figure S3b shows the comparisons with observations. Though the disparity between observations and simulations continues, performance statistics and variation in spatial patterns are reversed in the second set. For example, BAM AMIC simulated CLDF over Northern Africa, Central Asia, the North Atlantic, West Coast and Southern Australia is comparatively less positively biased towards MODIS observation (b,b′,b″). Statistically, the NMB for BAM AMIC is lower (31%) compared to BAM CTRL (36%), and the correlation is better (0.33 against 0.25). Simulated COD over high latitudes in both hemispheres is overpredicted with NMB 356% and RMSE 138.88 when no aerosols are present, and 237% and 97.23 respectively when aerosols are present. The simulated LWP is underpredicted but BAM CTRL simulated LWP has low NMBs (−39%).

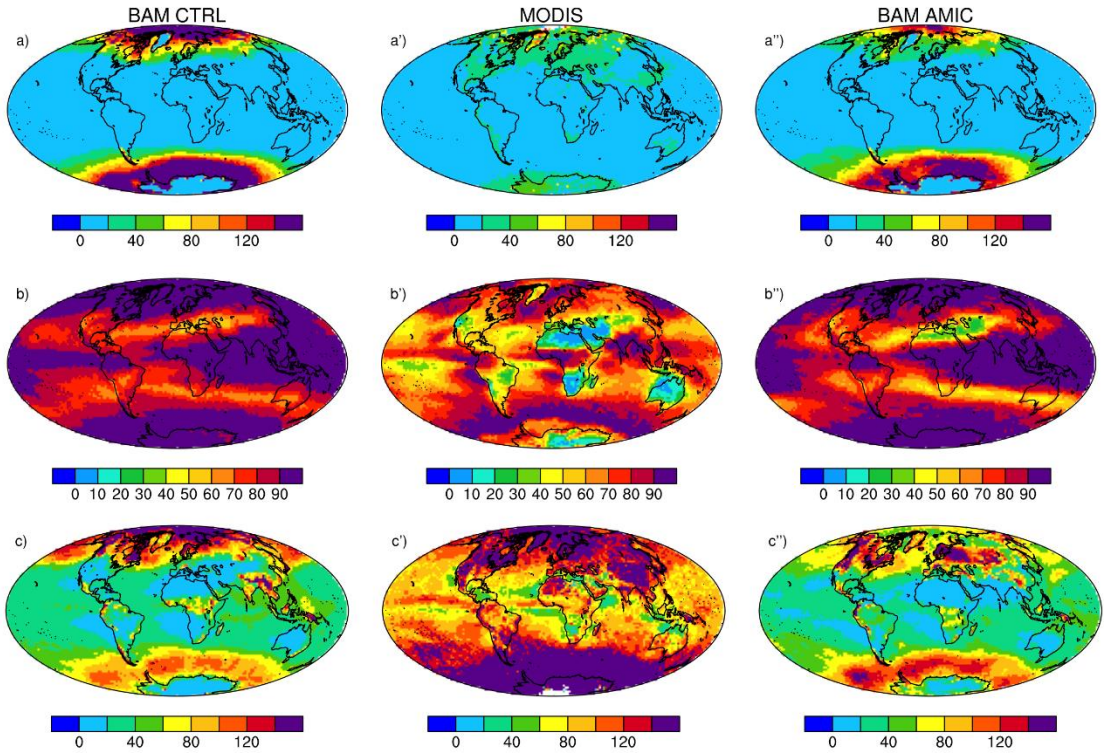

Figure S3. b: Similar to Figure S3a but for JAS2019.

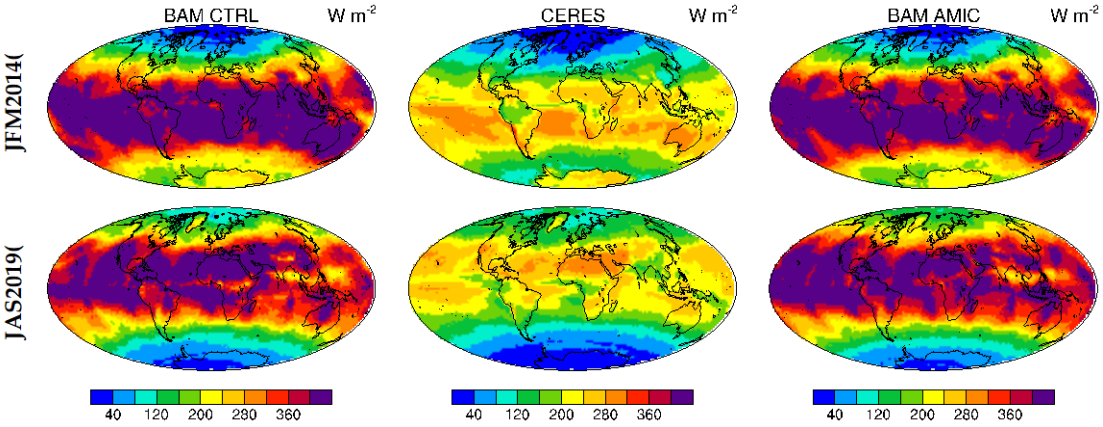

Figure S4. Model evaluation of downward shortwave radiation for JFM2014 and JAS2019. Simulated JFM means from BAM CTRL (left column) and BAM AMIC (right column) are compared with CERES satellite observations (middle column) corresponding to similar period.

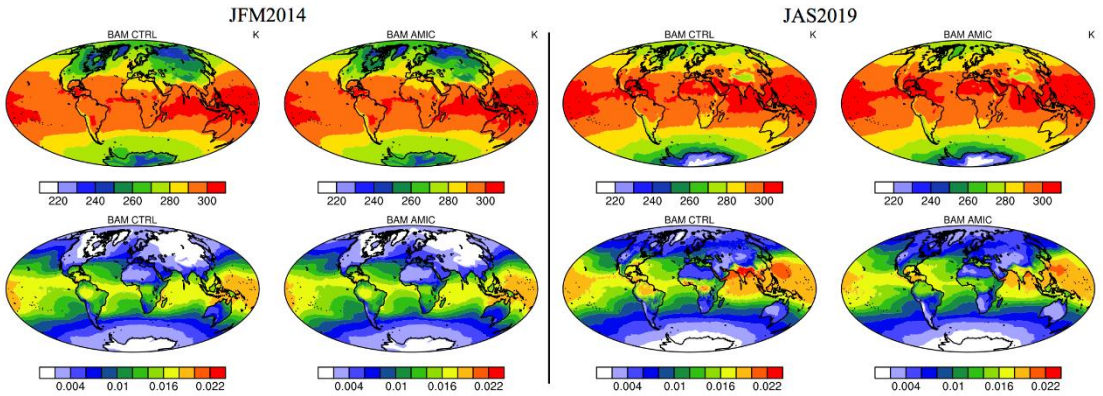

Figure S5. 2-m temperature (top panel) and specific humidity (bottom panel) in BAM CTRL and BAM AMIC simulations averaged for the periods – JFM2014 and JAS2019.